Chemical Physics Letters 460 (2008) 432–437

Contents lists available at ScienceDirect

Chemical Physics Letters

journal homepage: www.elsevier.com/locate/cplett

Structural variations and hydrogen storage properties of Ca_5Si_3 with Cr_5B_3-type structure

Hui Wu [a,b,*], Wei Zhou [a,b], Terrence J. Udovic [a], John J. Rush [a,b], Taner Yildirim [a,c]

[a] NIST Center for Neutron Research, National Institute of Standards and Technology, 100 Bureau Dr., Gaithersburg, MD 20899-6102, United States
[b] Department of Materials Science and Engineering, University of Maryland, College Park, MD 20742-2115, United States
[c] Department of Materials Science and Engineering, University of Pennsylvania, 3231 Walnut Street, Philadelphia, PA 19104-6272, United States

ARTICLE INFO

Article history:
Received 22 April 2008
In final form 7 June 2008
Available online 12 June 2008

ABSTRACT

The structure and phase variation of Ca_5Si_3 upon hydrogenation were systematically investigated using combined neutron powder diffraction (NPD), neutron vibrational spectroscopy (NVS), and first-principles calculations. The hydrogen absorption equilibrium was first attained with formation of $Ca_5Si_3H(D)_{0.53}$ (*I*4/*mcm*) with H exclusively located in Ca_4-tetrahedral sites. More hydrogen absorbed into the system under higher pressure leads to dissociations into CaH_2 (an amorphous hydride at higher pressures) and CaSi. The hydrogen-induced formation of an amorphous phase under higher pressures is very unusual in Cr_5B_3-type compounds and the observed formation of CaH_2 upon hydrogen absorption confirmed the proposed composition equilibrium between A_5Tt_3 (A = Ca, Sr; Tt = Si, Ge, Sn) and AH_2.

1. Introduction

Extensive efforts are being made to develop sustainable and clean energy sources to replace the use of carbon-based fuels. Successful development of hydrogen as a primary fuel will simultaneously reduce dependence on fossil fuel and emissions of greenhouse gases and pollutants. One of the major challenges to realize a future hydrogen economy is the lack of suitable hydrogen storage materials with the operating storage requirements for fuel-cell vehicular applications in the range of 0.1–1 MPa and 298–473 K [1]. Metal hydrides are an important family of materials that can be potentially used for safe, efficient and reversible on-board hydrogen storage. Particularly, intensive interest has been focused on light-weight metal hydrides such as LiH and MgH_2 due to their relatively high hydrogen-storage densities. However, most of these hydrides have rather slow absorption kinetics, relatively high thermal stability, and/or problems with the reversibility of hydrogen absorption/desorption cycling. Therefore, so far there is no such candidate system that can meet all the requirements simultaneously.

Recently, alloying with Si has been shown to effectively destabilize LiH and MgH_2 at significantly lower temperatures by forming Li–Si and Mg–Si intermetallic compounds upon dehydrogenation [2]. These Si-alloying studies have been extended to CaH_2 and the hydrogen-storage properties of the resulting Ca–Si intermetallic compounds [3–5]. Among them, CaSi was found to reversibly absorb and desorb hydrogen in a moderate temperature range of 473–573 K [3]. Ca_2Si shows even more rapid absorption kinetics with the formation of a reversible amorphous hydride phase in the temperature range of 473–523 K [5]. These prior studies motivated us to investigate hydrogen storage properties and structural variations upon hydrogenation/dehydrogenation of Ca_5Si_3, another important intermetallic phase in the Ca–Si system.

The crystal structure of Ca_5Si_3, as well as other alkaline-earth tetralides, A_5Tt_3 (A = Ca, Sr, and Ba; Tt = Si, Ge, Sn and Pb), belongs to the frequently encountered tetragonal Cr_5B_3-type structure, which features an equal number of monomeric and dimeric anions so that the divalent cations formally meet the structure criterion[6] for Zintl phases, $(A^{2+})_5(Tt_2^{6-})(Tt^{4-})$, in terms of oxidation states. The presence of a significant A_4-tetrahedral cavity in this structure type allows a ready incorporation of small quantities of hydrogen or fluorine into the structure, resulting in oxidation of the substrate. The oxidation of A_5Tt_3 phases to hydride or fluoride derivatives has been shown to have significant impact on their electronic and magnetic properties [7,8]. In the present study, we will focus mainly on the structure variations upon hydrogenation and the resulting hydrogen storage properties.

In our earlier studies in CaSi and Ca_2Si [4,5], we have developed a method of preparing crystalline metal-silicide phases upon the dehydrogenation of ball milled CaH_2 and Si mixtures. Using this method, the intermetallic phases can be synthesized at temperatures significantly lower than the conventional metal-melt method [9,10]. Our hydrogenation studies were undertaken on samples prepared by this method. In this Letter, we address the structural behavior and absorption properties of the Ca_5Si_3 system using combined neutron powder diffraction (NPD), neutron vibrational

* Corresponding author. Address: NIST Center for Neutron Research, National Institute of Standards and Technology, 100 Bureau Dr., Gaithersburg, MD 20899-6102, United States. Fax: +1 301 921 9847.
E-mail address: huiwu@nist.gov (H. Wu).

0009-2614/$ - see front matter © 2008 Elsevier B.V. All rights reserved.
doi:10.1016/j.cplett.2008.06.018

spectroscopy (NVS) and first-principles calculations. From the refinement of NPD data on a deuterided sample, we discuss the crystal structure of $Ca_5Si_3H_x$ and correlate its detailed structural features with other hydrogenated Cr_5B_3-type alkaline-earth tetralides. Upon hydrogenation at higher pressure or higher temperature, complete hydrogenation of Ca_5Si_3 yielded a maximum hydrogen uptake of 1.4 wt% rather than 0.35 wt% assuming the formation of fully hydrogenated Ca_5Si_3H. Extra hydrogen absorbed into the system leads to the formation of CaH_2 and an unexpected amorphous phase. To the best of our knowledge, this is the first reported observation of hydrogen-induced amorphization in an intermetallic compound with a Cr_5B_3-type structure.

2. Experimental section

A Ca_5Si_3 powder sample was synthesized by the following procedures. Stoichiometric 5:3 amounts of CaH_2 (Aldrich [11], 99.9%) and Si (Alfa Aesar 99.999%) powders were mixed under one atmosphere He gas via ball milling with a Fritsch Pulverisette 7 planetary mill at 400 rpm for 30 min. The mixture was then heated under dynamic vacuum for 10 h at 873 K to remove H_2. The product was ground again in an agate mortar with a pestle in a He-filled glovebox for further measurements. Using this method, the formation temperature of the metal-silicide phase, Ca_5Si_3, can be decreased by ≈500–550 K compared to the conventional metal-melt method [9]. Hydrided and deuterided samples were prepared using this Ca_5Si_3 by direct reaction with gas-phase H_2 and D_2 (99.999%), respectively, at various pressures and temperatures as detailed in the next section. All dehydrogenation and hydrogenation reactions were carried out in Mo envelopes that were sealed in a stainless steel tube and heated either under dynamic vacuum or under gas pressure in a conventional tube furnace, depending on the target. All reagents and products were handled in an ultra-pure He-filled glovebox.

All neutron scattering measurements were performed at NIST Center for Neutron Research (NCNR). The NPD data were collected using the BT1 high-resolution powder diffractometer [12] with the Cu(3 1 1) monochromator at a wavelength of 1.5403(2) Å and an in-pile collimation of 15 min of arc. Data were collected over the 2θ range of 3–168°. Rietveld structural refinements were done using the GSAS package [13]. The neutron vibrational spectra were measured using the BT-4 Filter-Analyzer Neutron Spectrometer [14] with the Cu(2 2 0) monochromator under conditions that provided full-width-at-half-maximum energy resolutions of 2–4.5% of the incident energy over the range probed. Hydrogen contents of samples were measured using the neutron prompt-γ activation analysis (PGAA) facility [15]. A pure CaH_2 sample was used as the standard material to normalize γ-ray intensities. Deuterium content was determined by gravimetric measurements.

First-principles calculations were performed within the plane-wave implementation of the generalized gradient approximation to density functional theory (DFT) using the PWSCF package [16]. We used a Vanderbilt-type ultrasoft potential with Perdew-Burke-Ernzerhof exchange correlation. A cutoff energy of 400 eV and a $4 \times 4 \times 4$ k-point mesh were found to be enough for the total energy to converge within 0.5 meV/atom and 0.005 eV/Å. Structure optimizations were performed with respect to lattice parameters and atomic positions. The phonon calculations were conducted with the optimized structure using the supercell method with finite difference [17,18].

3. Results

A single-phase Ca_5Si_3 alloy is formed upon dehydrogenation of the ball milled CaH_2/Si mixture in a ratio of 5:3 at 873 K. The NPD pattern (Fig. 1) of this alloy contains only reflections of a Cr_5B_3-type tetragonal structure (space group $I4/mcm$) with refined lattice parameters $a = 7.64988(9)$ Å, and $c = 14.8268(3)$ Å, which agrees well with previous reported values [8,10]. Annealing this sample at 573 K under 0.1 MPa H_2 resulted in an equilibrium composition $Ca_5Si_3H_{0.5}$ as determined by the PGAA technique. Refinement of the NPD data (Fig. 1) from the deuterided composition at the same conditions yielded a similar $I4/mcm$ tetragonal structure with the reduced lattice parameters, $a = 7.6394(2)$ Å and $c = 14.7935(1)$ Å, and a deuterium occupancy of 0.530(1). The refined lattice parameters, fractional coordinates, site occupancies, thermal parameters,

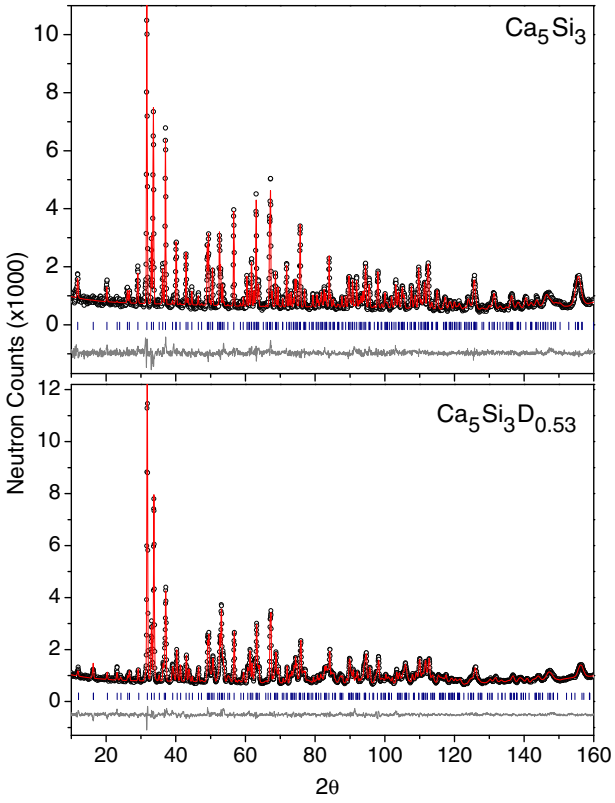

Fig. 1. Experimental (circles), calculated (red line), and difference (grey line) NPD profiles for Ca_5Si_3 (top panel) and $Ca_5Si_3D_{0.53}$ (bottom panel) at 295 K. Vertical bars indicate the calculated positions of Bragg peaks for Ca_5Si_3 (in top panel) and $Ca_5Si_3D_{0.53}$ (in bottom panel), respectively. (For interpretation of color in Fig. 1, the reader is referred to the web version of this article.)

Table 1
Crystallographic parameters for Ca_5Si_3 and $Ca_5Si_3D_{0.53}$

	Ca_5Si_3	$Ca_5Si_3D_{0.53}$
T (K)	295 K	295 K
Radiation type	Neutron	
Diffractometer	BT1, HRPD (Cu(311) monochromator, $\lambda = 1.5403(2)$)	
Measured 2θ range (°)	3-165	
Measured 2θ step size (°)	0.05	
Cell Setting, Space group	I4/mcm (No. 140)	I4/mcm (No. 140)
a (Å)	7.64988(9)	7.6394(2)
c (Å)	14.8268(3)	14.7935(2)
V (Å^3)	867.679(20)	863.325(25)
Z	4	4
R_{wp}	0.0463	0.0447
R_p	0.0382	0.0352
R_F	0.0541	0.0616
χ^2	1.025	1.748
No. of constraints	No constraints and restraints used	

Table 2
Structural parameters for Ca_5Si_3 and $Ca_5Si_3D_{0.53}$

Atom	Site	Occupancy	x	y	z	U_{11}	U_{22}	U_{33}	U_{12}	U_{13}	U_{23}
Ca_5Si_3											
Ca1	4*c*	1.00	0	0	0	0.99(4)	U_{11}	2.98(2)	0	0	0
Ca2	16*l*	1.00	0.1785(1)	*x* + 1/2	0.14079(9)	1.28(4)	U_{11}	1.5(1)	−0.04(5)	−0.19(4)	U_{13}
Si1	4*a*	1.00	0	0	0.25	1.3(1)	U_{11}	1.6(1)	0	0	0
Si2	8*h*	1.00	0.3866(1)	*x* + 1/2	0	0.71(6)	U_{11}	1.1(1)	0.05(4)	0	0
$Ca_5Si_3D_{0.53}$											
Ca1	4*c*	1.00	0	0	0	1.06(2)	U_{11}	3.41(5)	0	0	0
Ca2	16*l*	1.00	0.1712(2)	*x* + 1/2	0.1452(1)	1.33(4)	U_{11}	2.0(1)	−0.01(4)	−0.11(3)	U_{13}
Si1	4*a*	1.00	0	0	0.25	1.4(1)	U_{11}	1.6(1)	0	0	0
Si2	8*h*	1.00	0.3878(2)	*x* + 1/2	0	0.72(5)	U_{11}	1.7(1)	−0.2(1)	0	0
D	4*b*	0.53(1)	0	0.5	0.25	1.5(5)	U_{11}	1.7(3)	0	0	0

Table 3
Selected Interatomic Distances (Å) in Ca_5Si_3 and $Ca_5Si_3D_{0.53}$

Atom 1–Atom 2	Ca_5Si_3	$Ca_5Si_3D_{0.53}$
Ca1–Ca2 (8×)	3.50299(1)	3.5544(1)
Ca2–Ca2 (4×)	3.9781(1)	4.0049(5)
Ca2–Ca2 (2×)	4.23645(9)	4.0567(2)
Ca2–Ca2 (1×)	3.8629(1)	3.6992(1)
Ca2–Ca2 (1×)	4.1795(3)	4.2960(3)
Ca2–Ca2 (1×)	3.5847(3)	3.5374(3)
Si1–Ca1 (2×)	3.70671(9)	3.6984(2)
Si1–Ca2 (8×)	3.2446(9)	3.2285(3)
Si2–Ca1 (4×)	3.08635(8)	3.0841(2)
Si2–Ca2 (4×)	3.0985(1)	3.0828(3)
Si2–Ca2 (2×)	3.0721(2)	3.1766(4)
Si2–Si2 (1×)	2.43575(7)	2.4239(3)
D–Ca2 (4×)[a]	(2.520)	2.4134(2)

[a] To centroid of tetrahedron.

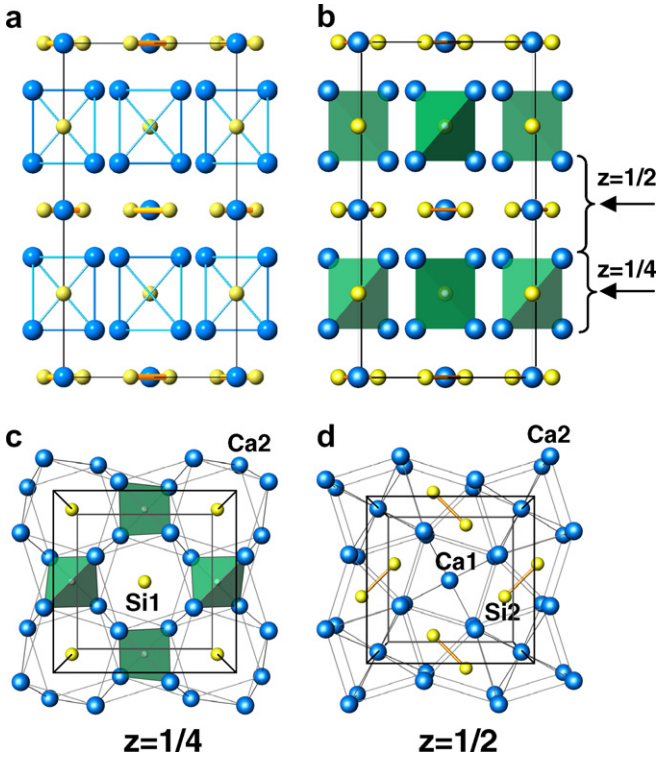

Fig. 2. (Top) [1 0 0] view of the tetragonal structures of (a) Ca_5Si_3 and (b) $Ca_5Si_3D_{0.53}$ with empty and filled Ca_4-tetrahedral cavities. (Bottom) [0 0 1] projection of the alternating portions in $Ca_5Si_3D_{0.53}$ structure: (c) centered at *z* = 1/2 or 0 and (d) centered at *z* = 1/4 or 3/4. The large blue and small yellow spheres are Ca and Si, respectively. The interstitial *D* is centered in the shaded $(Ca2)_4$-tetrahedra. (For interpretation of color in Fig. 2, the reader is referred to the web version of this article.)

and reliability factors for Ca_5Si_3 and $Ca_5Si_3D_{0.53}$ measured at 295 K are summarized in Tables 1 and 2. Table 3 lists important interatomic distances. The empty and hydrogenated Ca_5Si_3 tetragonal structures are illustrated in Fig. 2. The latter exhibits the characteristic feature of the hydrogenated Cr_5B_3-type structure: equally distributed Si monomers (at *z* = 1/4 and 3/4 layers) and dimers (at *z* = 0 and 1/2 layers) with different orientations, and interstitial tetrahedral cavities defined by Ca2 (16*l*) atoms around 4*b* sites. The $Ca_5Si_3D_{0.53}$ structure directly determined from the neutron data is comparable to the reported structure of $Ca_5Si_3F_{0.42}$ [8]. All D atoms occupy the single-type of tetrahedral interstitial sites (4*b*) defined by Ca2 (16*l*) atoms. Compared to that of the parent Ca_5Si_3, the lattice of $Ca_5Si_3D_{0.53}$ (Table 1) is contracted, which presumably originates from the metal-hydrogen bonding in the nominal tetrahedra $\bar{4}2m$ and the resulting shrinkage of the tetrahedral site (Table 3 last row). Such lattice contraction in the hydrides or fluorides compared to the empty parent alloys was also observed in other A_5Tt_3 compounds. Previous studies on $Ca_5Tt_3F_x$ indicated that *x* increases with Tt size, i.e. the occupancies of F are 0.42, 0.66, 0.89, in Ca–Si, Ca–Ge [8] and Ca–Sn [7] systems. Similary, a nearly full hydrogen occupancy was observed in Ca_5Sn_3D [7]. Therefore, a partially filled deuterium site in Ca_5Si_3 determined by the present study reasonably falls in line with previous observations.

Neutron vibrational spectroscopy was then employed to study the local chemical environment and the binding of the tetragonally coordinated H in the Ca_5Si_3H structure. Fig. 3 shows neutron vibrational spectra (NVS) collected on $Ca_5Si_3H_{0.5}$ and $Ca_5Si_3D_{0.53}$. As expected, the isotope shift for the same mode obeys the relation $E_H/E_D \approx \sqrt{2}$ due to the doubled isotopic mass for D compared to H. Both spectra show a vibrational doublet, consistent with a single-type of hydrogen site in the structure, in agreement with the NPD results.

To understand the spectra and correlate the observed phonon density of states with the refined crystal structures, we performed first-principles phonon calculations on Ca_5Si_3H. The phonon calculations were performed with the optimized structure using the supercell method with finite difference [18]. A cell of $1a \times 1b \times 1c$ was used and the full dynamical matrix was obtained from a total of 14 symmetry-independent atomic displacements (0.02 Å). The NV spectra of Ca_5Si_3H were computed for a $10 \times 10 \times 10$ *q*-point grid within the incoherent approximation with the instrumental resolution taken into account [19]. The primitive cell of Ca_5Si_3H contains two formula units (i.e., 18 atoms), giving rise to a total of 54 phonon branches with Γ $(q = 0) = 3[3A1g(R) + 2A1u + 3A2g + 6A2u(IR) + 2B1g(R) + 3B1u + 4B2g(R) + 1B2u + 9Eu(IR) + 6Bg(R)]$, where R and IR correspond to Raman- and infrared-active modes,

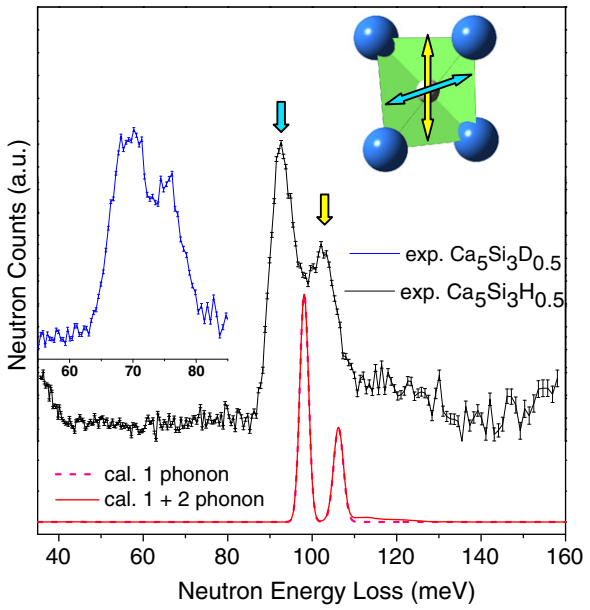

Fig. 3. NV spectra of $Ca_5Si_3H_{0.5}$ and $Ca_5Si_3D_{0.53}$ (inset) at 5 K. Calculated spectra for Ca_5Si_3H showing both 1 phonon (dotted line) and 1 + 2 phonon (solid line) contributions.

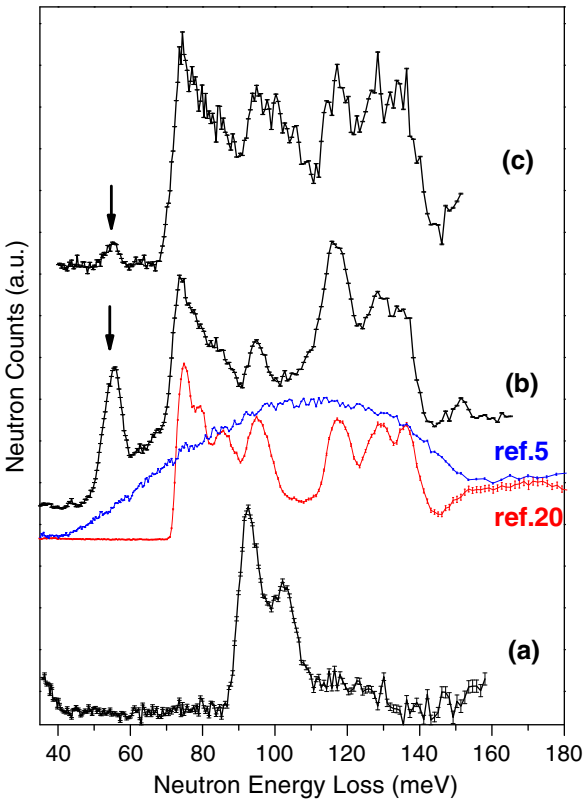

Fig. 4. Neutron vibrational spectra for $Ca_5Si_3H_x$ equilibrated at (a) 573 K and 0.1 MPa, (b) 573 K and 3 MPa and (c) 873 K and 0.1 MPa. Arrows point to the phonon modes from the unknown hydride phase(s). The spectra of CaH_2 (Ref. [20] and amorphous hydride phases (Ref. [5]) are also plotted for comparison.

respectively. The higher-energy vibrations are dominated by hydrogen displacements. The low-energy vibrations (< 40 meV) are largely associated with the displacements of Ca and Si and thus were not measured. Fig. 3 also compares the calculated phonon modes with the observed NV spectra. Calculations considering 1-phonon and (1 + 2) phonon contributions to the NV spectra yield similar spectra in the measured energy range. The observed doublet modes in the range of 85–110 meV in the NV spectra of $Ca_5Si_3H_{0.5}$ include six phonon modes ($1A_{2u} + 1B_{2g} + E_u + E_g$), all originated from H (4*b*) atoms in the Ca_4-tetrahedral sites. The higher-energy phonon band (including $1A_{2u} + 1B_{2g}$ modes) corresponds to the in-phase and out-of-phase vibrations of H along the c direction, and the lower band (including $E_u + E_g$ modes) is assigned to the in-phase and out-of-phase vibrations of H along the ⟨1 1 0⟩ direction. In Fig. 3 the measured spectra showed phonon bands with lower energies compared to the calculations, likely due to the partial filling of H sites in the actual structure with consequently weakened H-metal bonding. Nonetheless, the calculated phonon modes agree reasonably well with the observed NVS, and thus are consistent with the refined structure determined from the NPD data.

Upon hydrogenation of Ca_5Si_3 at higher pressure, the system showed some interesting and unexpected structural variations. Fig. 4 shows NV spectra for the samples upon hydrogenation under different pressures and annealing temperatures. Annealing at 573 K with a relatively high H_2 pressure, i.e. 3 MPa, produces an equilibrium composition of $Ca_5Si_3H_{4.41}$. The most prominent groups of phonon modes for this composition represent the hydrogen vibrations in calcium hydride (CaH_2) [20]. The spectrum of pure CaH_2 is shown for comparison. There is an additional strong peak observed in the lower-energy portion (50–60 meV), which is due to the dissociation of the alloy phase upon hydrogenation and was also present in the previous H_2-pressurized Ca_2Si system [5]. The third noticeable feature in the NV spectrum is the partial phonon mode smearing due to an amorphous phase component appearing in the hydrogenated products. Such hydrogenation induced amorphization (HIA) has been observed in the Ca_2Si system [5]. The spectrum of the amorphous hydride resulting from Ca_2Si hydrogenation [5] is also plotted for comparison. Similar to the Ca_2Si system, the amorphous component phase in the Ca_5Si_3 system was able to crystallize after an extended annealing at higher temperature (e.g. 600 K) under 0.1 MPa H_2. The small hydrogen overpressure was maintained in order to prevent any loss of H content from the amorphous phase during the extended heat treatment. Crystallization was evidenced by the well-defined diffraction peaks in the NPD pattern collected on a similarly prepared deuterided sample $Ca_5Si_3D_{4.4}$. Careful analysis of these crystalline reflections revealed a mixture of CaD_2 (38.8%) and CaSi (61.2%), but no $Ca_5Si_3D_x$ phase. This indicated that the $Ca_5Si_3D_x$ phase decayed into CaD_2 and CaSi after hydriding under high pressures. The diffraction pattern also includes a small amount of unknown calcium silicide phase as evidenced by the difference profile. The reflections of the unknown phase do not match the diffraction pattern of any known Ca silicide compound. Further work on this phase is in progress to determine its composition and structure, as well as to better understand the overall destabilization processes.

Annealing at higher temperature while keeping the small pressure unchanged, i.e. 0.1 MPa at 873 K, also generates a similar equilibrium composition, $Ca_5Si_3H_{4.08}$. The vibrational spectrum of this sample is again dominated by CaH_2. Small peaks due to the above mentioned unknown hydride phase are also observed. However, this spectrum shows little evidence of contributions from amorphous phases, as evidenced by the fairly flat base line, as observed for that of pure crystalline CaH_2. Apparently, high temperature can enhance the absorption amount with relatively lower pressure, similar to the results of high pressure at lower temperature, but it will also effectively suppress the amorphization process. NPD data collected on deuterium-loaded Ca_5Si_3 samples under the same treatment conditions revealed a multiphase mixture of CaD_2

Table 4
Summary of $Ca_5Si_3H_x$ samples prepared under different H_2 (D_2) pressures

Compositions	Treatment	Major phases	Phase Fraction			Other phase	Detect methods
			a (Å)	*b* (Å)	*c* (Å)		
$Ca_5Si_3H_{0.5}$	573 K	$Ca_5Si_3H_{0.4}$	N/A			-	NVS, PGAA
$Ca_5Si_3D_{0.530(1)}$	0.1 MPa H_2/D_2	$Ca_5Si_3D_{0.530(1)}$ (*I*4/*mcm*)	7.6394(2)		14.7054(1)		NPD
$Ca_5Si_3H_{4.41}$	573 K	CaH_2; amorphous	–			unknown hydrides	NVS, PGAA
$Ca_5Si_3D_{4.4}$	3 MPa H_2/D_2	CaD_2 (*Pnma*)	[F_{CaD2} = 38.8(3)%]				NPD
			5.9668(5)	3.6073(3)	6.8219(6)		
		CaSi (*Cmcm*)	[F_{CaSi} = 61.2(2)%]				
			4.550(4)	10.79(1)	3.855(4)		
$Ca_5Si_3H_{4.08}$	873 K	CaH_2	–			unknown hydrides	NVS, PGAA
$Ca_5Si_3D_{4.1}$	0.1 MPa H_2/D_2	CaD_2 (*Pnma*)	[F_{CaD2} = 33.6(2)%]				NPD
			5.969(1)	3.6146(6)	6.815(1)		
		CaSi (*Cmcm*)	[F_{CaSi} = 66.4(3)%]				
			4.543(1)	10.962(4)	3.824(1)		

[33.6%], CaSi [66.4%] and small amounts of unknown phases as observed previously, consistent with the NVS results. The products of Ca_5Si_3 under various treatment conditions are summarized in Table 4.

All the products after hydrogenation can be recycled. After dehydrogenating at 873 K, a single-phase intermetallic compound Ca_5Si_3 was recovered (see Supplementary material), which confirms the reversible hydrogenation of this system.

4. Discussion

In order to have a better understanding of the Ca_5Si_3 phase and its hydrogenation process, in this section, we will compare the structure of $Ca_5Si_3H_x$ with its fluoride analogue and other A_5Tt_3 hydrides/fluorides, and discuss the degradation process of Ca_5Si_3 alloy upon hydrogenation.

As mentioned in the introduction, the crystal structure of Ca_5Si_3, as well as other Cr_5B_3-type alkaline-earth tetralides A_5Tt_3, features an equal number of monomeric and dimeric anions and the presence of an A_4-tetrahedral cavity. A small quantity of hydrogen or fluorine can be readily incorporated into the structure without a change in the symmetry, forming a hydride or fluoride phase via heating the alloy under 0.1 MPa or less pressure at moderate temperatures. In some extreme cases, the binary alloy does not even exist and can only be stabilized through interstitial binding, i.e. $Ca_5Sn_3H_x$ and $Sr_5Pb_3F_x$. Apparently, the amount of hydrogen or fluorine incorporated depends on the size of such cavities and the binding strength between H(F), alkaline-earth cations (A2-site), and the tetralide dimers. In Fig. 5, the known $A_5Tt_3D_x$ and $A_5Tt_3F_x$ compounds with the refined deuteride and fluoride occupancies are mapped as a function of tetralide anion radii. Variations in the size of tetrahedral site (e.g. A2-*Z* distance) with Tt radius changes are also plotted for Ca_5Tt_3 and $Ca_5Tt_3Z_x$. In general, the content of F or H in the structure increases with the size of Tt given the same radius of A (e.g. Ca). This is a fairly straightforward size effect, as the tetrahedral cavity increases with increasing Tt at fixed A (green open triangle line in Fig. 5).[1] The effect of binding H^- or F^- relative to the empty binary version reduces the sizes of the tetrahedral cavity (Fig. 5, black open square and red open circle lines), the decrements of which are reasonably proportional to the H or F content (Fig. 5, solid square and red solid circle lines). Substitution of F in the tetrahedral cavity results in smaller occupancy and hole size decrements than those for H at fixed A and Tt, which is consistent with their comparative radii. From the present comparison between

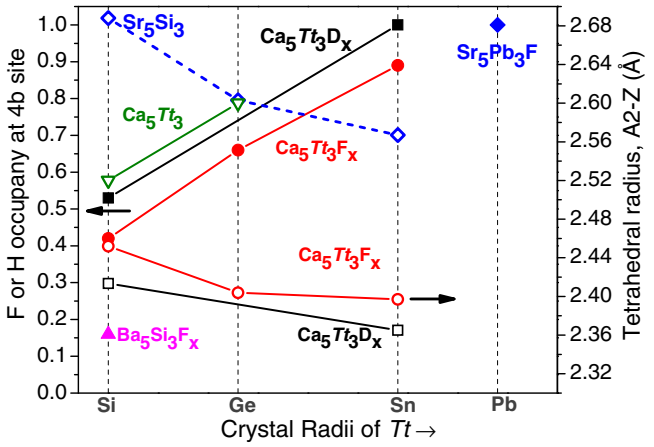

Fig. 5. Schematic illustration of the effect of Tt and A radii and the size of A_4-tetrahedral cavities on *Z* occupancies in $A_5Tt_3Z_x$ (*Z* = H, F). Solid symbols indicate the determined occupancies of Z (left axis); open symbols represent the calculated radius of tetrahedral cavities (right axis). The data for these compounds except Ca_5Si_3 and $Ca_5Si_3D_{0.53}$ are from Refs. [7,8,21,22].

the empty and filled A_4-tetrahedral sizes with Tt radii and H or F content, the questionable trend of the reduced empty Sr_4-tetrahedral hole size with larger Tt in Sr_5Tt_3 (Fig. 5, blue open diamond line) suggests probable hydrogen contamination for the reported Sr_5Ge_3 [21] and Sr_5Sn_3 [22]. Previous comparison of the positional data in clean and contaminated Sr_5Si_3 [22] suggested this possible formation of hydrides, and the observed cell volume decrements between Sr_5Tt_3 and $Sr_5Tt_3H_x$ were found to be proportional to H content [8], which are consistent with our argument.

Upon binding H or F, the decrease in the top and bottom edges of $A(2)_4$-tetrahedra was observed to be directly coupled to a twist of the $A(2)_8$-antiprismatic surroundings about Tt1. Such effects also extend to the section of the structure that contains the Tt2 dimer and cause the increasingly anisotropic environment around the waist of the $Tt(2)_2$ dimer, which will split the degeneracies of the π levels on the dimers. Therefore, with increasing concentration of H or F, the interstitials would withdraw more π^* electron density from the heavier and weaker dimers and the Tt2–Tt2 bond lengths in the dimers would generally shorten as π^* electrons are removed. For binary A_5Tt_3 with empty tetrahedra for larger Tt (Tt = Sn and Pb), the absence of interstitial binding will yield too short distances between the A2 sites around the larger Tt_2, which would consequently destabilize the structure. As a result, the

[1] For interpretation of color in Fig. 5, the reader is referred to the web version of this article.

binary version of Ca_5Sn_3 and Sr_5Pb_3 has never been reported, and only examples of $Ca_5Sn_3Z_x$ and Sr_5Pb_3F ternaries occur.

On the other hand, Fig. 5 also indicates that the occupancy of F decreases with increasing size of A at fixed Tt. This is in contrast to their tetrahedral hole sizes. Considering our studies in Ca_5Si_3 and its hydrogenation products at various pressures, we propose as a possible explanation that the H content in the $A_5Tt_3H_x$ structure is related to its equilibrium with AH_2 (see the discussion below). The equilibrium would move toward the formation of AH_2 with higher H_2 pressure (more H), greater electropositivity of A (stronger A–H bond), and increasing temperatures.

We next discuss the hydrogen-induced degradation behavior in Ca_5Si_3. The parent Cr_5B_3-type lattice is essentially maintained with hydrogen atoms exclusively occupying Ca_4 tetrahedral sites under 0.1 MPa at 573 K. Such a Cr_5B_3-type structure will collapse and dissociate under higher pressures or at higher temperatures. Considering the NV spectrum of $Ca_5Si_3H_x$ (Fig. 3) and refined NPD data for the hydrogenation products (Table 4 and Supplementary material), where the crystalline CaH_2 phase can be clearly detected, Ca_5Si_3 presumably decomposed through following route:

Ca_5Si_3 (or $Ca_5Si_3H_{0.5}$) + $2H_2 \rightarrow 2CaH_2 + 3CaSi$ (+ amorphous hydride phase at $P = 3$ MPa)

The hydrogen-induced amorphization (HIA) phenomenon is frequently observed in families of intermetallic compounds with certain crystal structures such as laves phases. The Ca_5Si_3 phase does not belong to any of these structure families, however, the current system satisfies the general requirements [23] described for amorphous or metal-glass formation in a solid state reaction: (i) at least a ternary system, (ii) a large disparity in the atomic diffusion rates of two of the species, and (iii) the absence of a polymorphic crystalline alternative as a final state. Therefore, the formation of an amorphous hydride phase upon relatively higher pressure hydrogenation ($P = 3$ MPa in the present study) can be explained by the previously proposed 'chemical frustration effect', where the glassy hydride would appear to be a metastable alternative of the crystalline phase because it does not require the interdiffusion of metal species (i.e., Ca and Si), which is much slower than the highly mobile hydrogen atoms with increasing H_2 pressure [23,5]. In addition, in Ca_5Si_3 the amorphization under high pressure did not change below ≈573 K with hydrogenation time. In other words, the amorphous phase could still be observed even after hydrogenating a Ca_5Si_3 sample for a long period, e.g., 8–10 h, at this temperature. Thus we believe this chemical frustration effect, rather than kinetic effects, is primarily responsible for the transition to the amorphous state.

The composition of final product ($2CaH_2 + 3CaSi$) is in good agreement with the stoichiometries of the high pressure ($Ca_5Si_3H_{4.41}$) and high temperature ($Ca_5Si_3H_{4.08}$) products determined by PGAA. The hydrogen content more than four may be contributed by the unknown hydride phase as observed in the NPD data. Nonetheless, the observed formation of CaH_2 confirms our proposed absorption equilibrium between A_5Tt_3 and AH_2.

The facile absorption behavior and the complete reversibility make Ca_5Si_3 an intriguing system for hydrogen storage, particularly if the absorption/desorption temperatures could be further reduced by the use of dopants and /or catalysts. In that sense, the current system can aid us in designing new hydride materials with lighter metal substituents and thus higher storage capacities.

5. Conclusions

The structure and phase variation of Ca_5Si_3 alloy upon hydrogenation process were systematically investigated using combined NPD, NVS and first-principles calculations. Upon hydriding under 0.1 MPa at 573 K the absorption equilibrium was attained with the formation of a Cr_5B_3-type structure $Ca_5Si_3H(D)_{0.53}$ ($I4/mcm$, No. 140) with H exclusively located in Ca_4-tetrahedral sites. From the refined NPD data, $Ca_5Si_3D_{0.53}$ shows a contraction in cell dimension and Ca_4-tetrahedral cavity size compared to Ca_5Si_3. Our refined structures also indicate the changes in positional parameters and the resulting complicated relationships among them with the interstitial binding, which is primarily responsible for the oxidation state, electronic structure, bonding strength, and stability of the structures. Upon hydrogenation under higher pressures (i.e., 3 MPa, 573 K) or higher temperature (i.e., 873 K, 0.1 MPa) Ca_5Si_3 absorbs hydrogen and dissociates into CaH_2 (amorphous hydride at high pressure) and CaSi. Such structure behavior upon hydrogenation has not been previously reported in any A_5Tt_3-type intermetallic compounds (A = Ca, Sr; Tt = Si, Ge, Sn). The observed formation of CaH_2 upon hydrogen absorption confirms the proposed composition equilibrium between A_5Tt_3 and AH_2. The hydrogen-induced formation of an amorphous phase at higher pressures is very unusual in intermetallic compounds with the Cr_5B_3-type structure, but could be rationalized as previously described in Ca_2Si.

Acknowledgments

This work was partially supported by DOE through EERE Grant No. DE-AI-01-05EE11104 (T.J.U.) and BES Grant No. DE-FG02-98ER45701 (T.Y.).

Appendix A. Supplementary material

NPD patterns of hydrogenation products of Ca_5Si_3 under 30 MPa at 573 K and under 1 MPa at 873 K. Supplementary data associated with this article can be found, in the online version, at doi:10.1016/j.cplett.2008.06.018.

References

[1] http://www.eere.energy.gov/.
[2] J.J. Vajo, F. Mertens, C.C. Ahn, R.C. Bowman Jr., B. Fultz, J. Phys. Chem. B 108 (2004) 13977.
[3] M. Aoki, N. Ohba, T. Noritake, S. Towata, Appl. Phys. Lett. 85 (2004) 387.
[4] H. Wu, W. Zhou, T.J. Udovic, J.J. Rush, T. Yildirim, Phys. Rev. B 74 (2006) 224101.
[5] H. Wu, W. Zhou, T.J. Udovic, J.J. Rush, Chem. Mater. 19 (2007) 329.
[6] T. Hughbanks, T. Fehlner (Eds.), Inorganometallic Chemistry, Plenum Press, New York, 1992, p. 291.
[7] E.A. Leon-Escamilla, J.D. Corbett, Inorg. Chem. 40 (2001) 1226.
[8] E.A. Leon-Escamilla, J.D. Corbett, J. Solid State Chem. 159 (2001) 149.
[9] V.B. Eisenmann, H. Schaefer, A. Weiss, Z. Anorg. Allg. Chem. 391 (1972) 241.
[10] P. Manfrinetti, M.L. Fornasini, A. Palenzona, Intermetallics 8 (2000) 223.
[11] Certain commercial suppliers are identified in this Letter to foster understanding. Such identification does not imply recommendation or endorsement by the National Institute of Standards and Technology, nor does it imply that the materials or equipment identified are necessarily the best available for the purpose.
[12] J.K. Stalick, E. Prince, A. Santoro, I.G. Schroder, J.J. Rush, In: D.A. Neumann, T.P. Russell, B.J. Wuensch, (Eds.), Neutron Scattering in Materials Science II, Mat. Res. Soc. Symp. Proc. vol. 376, Materials Research Society, Pittsburgh, PA, 1995, p. 101.
[13] A.C. Larson, R.B. Von Dreele, General Structure Analysis System, Report LAUR 86-748. Los Alamos National Laboratory, NM, 1994.
[14] T.J. Udovic, D.A. Neumann, J. Leão, C.M. Brown, Nucl. Instrum. Methods Phys. Res., Sect. A 517 (2004) 189.
[15] R.M. Lindstrom, J. Res. Natl. Inst. Stand. Technol. 98 (1993) 127.
[16] Baroni, S.; Dal Corso, A.; de Gironcoli, S.; Giannozzi, P. http://www.pwscf.org.
[17] G. Kresse, J. Furthmuller, J. Hafner, Europhys. Lett. 32 (1995) 729.
[18] T. Yildirim, Chem. Phys. 261 (2000) 205.
[19] G.L. Squires, Introduction to the Theory of Thermal Neutron Scattering, Dover, New York, 1996.
[20] H. Wu, W. Zhou, T.J. Udovic, J.J. Rush, T. Yildirim, J. Alloys Comp. 436 (2007) 51.
[21] R. Nesper, F. Zuercher, New Crystal Structures 214 (1999) 21.
[22] W. Doerrscheidt, A. Widera, H.Z. Schaefer, Naturforsch. B 32 (1977) 1097.
[23] X.L. Yeh, K. Samwer, W.L. Johnson, Appl. Phys. Lett. 42 (1983) 242.